Project funded by the European Commission under the 6th (EC) RTD Framework Programme (2002- 2006) within the framework of the specific research and technological development programme "Integrating and strengthening the European Research Area"

Project UpWind

Contract No.:
019945 (SES6)

"Integrated Wind Turbine Design"

RESEARCH REPORT
Electromagnetic Optimization of Direct-drive generators
(Deliverable No.: D 1B2.b.4)

AUTHOR:	Deok-je Bang[1], Henk Polinder[2]
AFFILIATION:	Delft University of Technology[1, 2]
ADDRESS:	Mekelweg4, 2628CD Delft, the Netherlands[1, 2]
TEL.:	+31 15 27 85791[1], +31 15 27 818441[2]
EMAIL:	d.j.bang@tudelft.nl[1], h.polinder@tudelft.nl[2]
FURTHER AUTHORS:	
REVIEWER:	Project members
APPROVER:	Jan Hemmelmann

Document Information

DOCUMENT TYPE	RESEARCH REPORT
DOCUMENT NAME:	Deliverable_1B2.b.4.pdf
REVISION:	1.0
REV.DATE:	14/10/2010
CLASSIFICATION:	R1: Restricted to project members
STATUS:	Approved

Abstract: The objective of this report is to determine the optimum parameters in a design of radial flux permanent magnet (RFPM) and transverse flux permanent magnet machines for large direct-drive wind turbines.
A determination of geometric parameters of both RFPM machine and TFPM machine is discussed in the report. A generalized electromagnetic design model is developed for both an RFPM machine and a TFPM machine. To validate the analytical design model of TFPM machines in no-load case, no-load induced voltage obtained from the analytical model is compared with the no-load voltages obtained through three-dimensional finite element analyses (3D FEA). The no-load voltage per pole pair in the analytical model is 8 % higher than the voltage obtained through 3D FEA. To validate the analytical model in the case with a load, the force obtained through the analytical model was compared with the force obtained by 3D FEA. At the nominal stator current, the force obtained by the analytical model is 10 % larger than the force obtained by the 3D FEA.
The analytical models developed in this report (Deliverable No.: D 1B2.b.4) will be used for a comparative design of PM generators for large direct-drive wind turbines in the final report (Deliverable No.: D 1B2.b.hp2).

Contents

1. Introduction 4
2. Main dimensions of PM machines 5
2.1 RFPM machine 5
2.2 TFPM machine 7
3. Generalization of magnetic circuit of PM machines 13
3.1 Linear model 13
3.2 Nonlinear model 15
3.3 Magnetic circuit modelling of PM machines 19
3.3.1 RFPM machine 19
3.3.2 TFPM machine 20
4. Verification of magnetic circuit analysis model 24
4.1 Verification of no-load case 24
4.1.1 Analysis model 24
4.1.2 Finite element analysis 27
4.2 Verification in the case with a load 27
5. Conclusions 29
References 30

STATUS, CONFIDENTIALITY AND ACCESSIBILITY									
Status				**Confidentiality**				**Accessibility**	
S0	Approved/Released	**X**		**R0**	General public			Private web site	X
S1	Reviewed	**X**		**R1**	Restricted to project members	X		Public web site	
S2	Pending for review			**R2**	Restricted to European. Commission			Paper copy	
S3	Draft for commends			**R3**	Restricted to WP members + PL				
S4	Under preparation			**R4**	Restricted to Task members +WPL+PL				

PL: *Project leader* **WPL:** *Work package leader* **TL:** *Task leader*

1. Introduction

The objective of this report is to determine the optimum parameters of radial flux permanent magnet (RFPM) and transverse flux permanent magnet (TFPM) machines for large direct-drive wind turbines. To achieve the objective, a generalized analytical model for various topologies of PM machines is developed and the model is validated through a comparison with finite element analyses (FEA).

In the review of PM machines in a previous report (Deliverable No.: D 1B2.b.1), it was discussed that surface-mounted radial flux permanent magnet (RFPM) machines have been mostly used for direct-drive applications. The flux-concentrating transverse flux permanent magnet (TFPM) machine has been discussed as a machine with high force density which results in reduction of volume and mass. Therefore, surface-mounted RFPM and flux-concentrating TFPM machines are chosen in the modelling of PM machines for direct-drive applications in this report.

A number of TFPM machine topologies have been proposed and discussed with a derivation of analytical models as discussed in a previous report, D 1B2.b.1. However, it seems rather difficult to apply those analytical models for various topologies of TFPM machines because the models are limited to specified topologies. Therefore, a generalized analytical model for various topologies of PM machines is developed in this report with the following outline.

Firstly, a determination of geometric parameters of both a surface-mounted RFPM machine and a flux-concentrating TFPM machine is discussed. Secondly, generalized electromagnetic circuit analysis models of both machines are developed. The models include nonlinear B-H curve characteristics of iron cores. Next, the proposed analysis model is verified through a comparison with finite element analyses.

The parameters of PM machines determined in this report will be used for the comparative design of PM generators for large direct-drive wind turbines in the final report (Deliverable No.: D 1B2.b.hp2).

2. Main dimensions of PM machines

This chapter concentrates on determining the main dimensions of both a surface-mounted radial flux permanent magnet (RFPM) machine and a flux-concentrating transverse flux permanent magnet (TFPM) machine.

2.1 RFPM machine

Figure 1 depicts a linearized cross-section of two poles of a surface-mounted radial flux permanent magnet (RFPM) machine with full pitch windings. In the figure, l_g is the air gap length, τ_s is the slot pitch, b_s is the stator slot width, b_t is the stator tooth width, h_{sy} is the stator yoke height, h_s is the stator slot height, l_m is the magnet length, h_{ry} is the rotor yoke height, b_p is the magnet width and τ_p is the pole pitch.

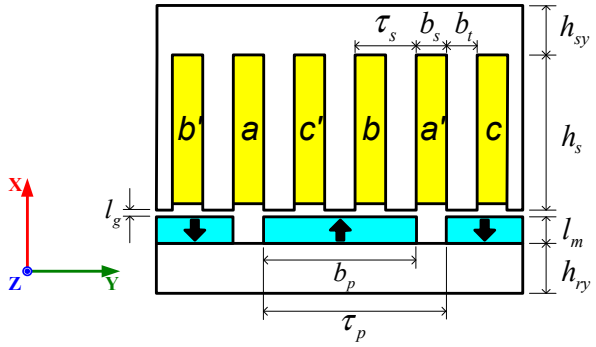

Figure 1: *A linearized cross-section of a surface-mounted RFPM machine*

In [1][2][3][4], the following dimensional parameters were discussed for direct-drive electric machines.

- Air gap length l_g of direct-drive wind generator was defined as a function of the air-gap diameter D_g, $l_g = D_g/1000$ in [1].
- Slot pitch τ_s of electric machine was discussed to choose between 19 mm and 38 mm in [2].
- Stator slot width b_s, tooth width b_t, magnet width b_p and slot pitch τ_s were defined as a function of the pole pitch τ_p in [2][3].
- The stator slot height h_s was discussed to choose between 3 and 7 times of the slot width b_s.
- Considering the flux paths and the continuity of flux, the stator yoke height h_{sy} and the rotor yoke height h_{ry} need to be larger than 1.5 times the tooth width b_t.

- In order to minimize total mass of direct-drive RFPM generators for 2, 3, 5 and 10 MW wind turbines, the optimum ratios of the axial length to the air-gap diameter $K_{rad} = l_s / D_g$ were chosen as 0.2, 0.23, 0.27 [4] and 0.3 [5], respectively.

Considering the above defined parameters, the dimensions and parameters of the RFPM machine are determined in TABLE 1.

TABLE 1
PARAMETERS AND DIMENSIONS OF RFPM MACHINES

Aspect ratio of generator	$K_{rad} = l_s / D_g$ [-]
Force density	$F_d = 40$ [kN/m^2]
Air gap diameter (Generator rotor diameter)	$D_g = \sqrt[3]{\frac{2T}{\pi K_{rad} F_d}}$ [m]
Axial length of generator	$l_s = \frac{2P_{gennom}}{\pi D_g^2 F_d \omega_m}$ [m]
Air gap length	$l_g = D_g / 1000$ [m]
Magnet height	$l_m = 2.5 l_g$ [m]
Stator diameter	$D_s = D_g + 2l_g$ [m]
Number of phases	$m = 3$ [-]
Stator slot pitch	$\tau_s = 0.033$ [m]
Number of slots per pole per phase	$q = 1$ [-]
Pole pitch	$\tau_p = mq\tau_s$ [m]
Number of pole pairs	$p = \pi D_g / 2\tau_p$ [-]
Rotor pole width	$b_p = 0.8\tau_p$ [m]
Stator slot width per slot pitch	$b_s / \tau_s = 0.45$ [-]
Stator slot width	$b_s = b_s / \tau_s \times \tau_s$ [m]
Stator tooth width	$b_t = \tau_s - b_s$ [m]
Stator slot height	$h_s = 5.3 b_s$ [m]
Stator yoke height	$h_{sy} = 2.22 b_t$ [m]
Rotor yoke height	$h_{ry} = h_{sy}$ [m]
Air gap area	$A_g = \pi D_g l_s$ [m^2]

2.2 TFPM machine

In a previous report (Deliverable No.: D 1B2.b.1), flux-concentrating double-sided transverse flux permanent magnet (TFPM) machines with single windings and C-core arrangement were discussed as the machines which offer a high torque density. Therefore, a flux-concentrating double-sided TFPM machine is chosen in the modelling of a TFPM machine.
Figure 2 depicts a linearized model and dimensional parameters of a double-sided single winding flux-concentrating TFPM machine with C-cores.

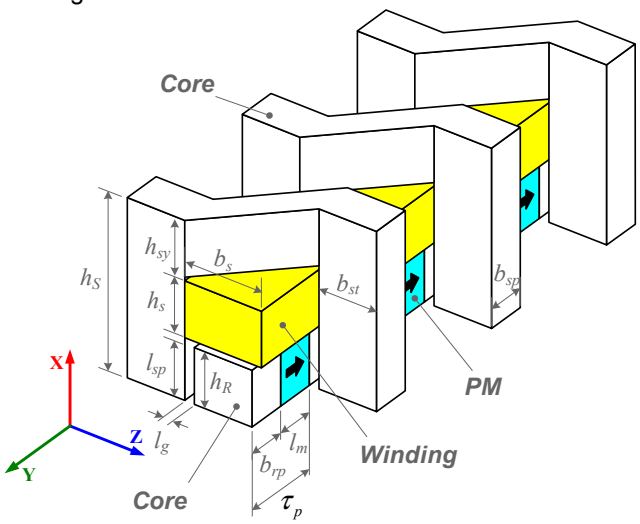

Figure 2: *A linearized double-sided single winding flux-concentrating TFPM machine with C-cores*

In Figure 2, l_g is the air gap length, b_s is the stator slot width, l_{sp} is the stator pole length, h_{sy} is the stator yoke height, h_s is the stator slot height, l_m is the magnet length, h_r is the rotor height, b_{sp} is the stator pole width, b_{rp} is the rotor pole width and τ_p is the pole pitch.

In order to determine the optimum electromagnetic dimensions and parameters of TFPM machines, two-dimensional (2D) static analyses of electromagnetic fields are done using a finite element analysis (FEA) software, the Flux2D. The static analysis model of electromagnetic fields is built as Figure 3. Dirichlet boundary condition with zero vector potential (***A***=0) is applied on the outer border lines of the model.

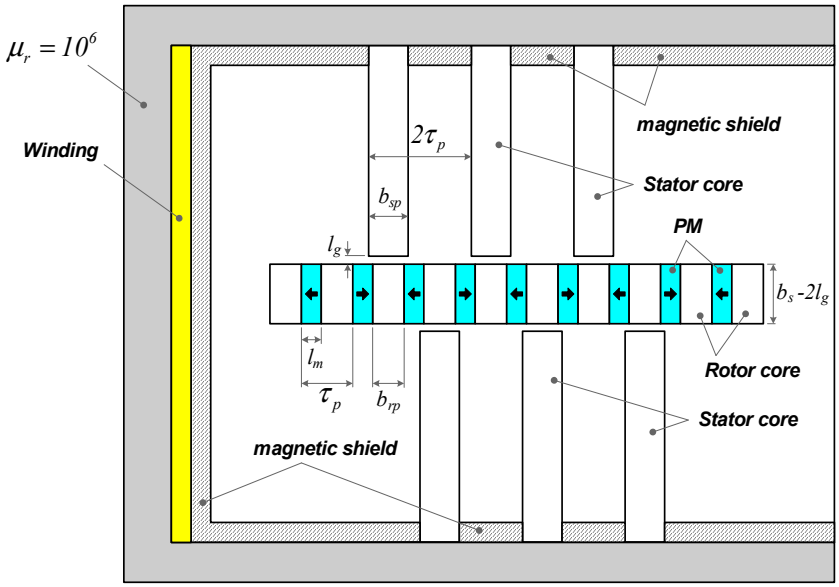

Figure 3: *Two-dimensional static analysis model of electromagnetic fields of TFPM machine*

The following processes and conditions are used to find optimum electromagnetic dimensions and parameters of TFPM machines by FEA.

(1) The remanent flux density and the relative recoil permeability of permanent magnets used in the model are B_{rm} =1.2 [T] and μ_{rm} =1.05 [-], respectively.

(2) The flux density and the magnetic field intensity curve of the iron core used in the analysis model is given in Figure 4. The iron core is 35PN380, an electrical steel model produced by a Korean steel company, the POSCO.

(3) The force density F_d of the machine is defined as an objective function to maximize under the electromagnetic dimensions and parameters given.

(4) In order to determine the electromagnetic dimensions of the TFPM machine achieving the maximum force density F_d, the magnet length l_m, the stator pole width b_{sp} and the pole pitch τ_p are used as variables in the FEA.

(5) The analyses to find the optimum ratios of the magnet length to the pole pitch (l_m/τ_p) and the stator pole width to the pole pitch (b_{sp}/τ_p) are done. In the analyses, the magneto-motive force mmf by current, the air-gap length l_g and the pole pitch τ_p are fixed to 3000 [AT], 1 [mm] and 20 [mm], respectively. Force densities F_d are calculated as a function of the magnet length l_m and the stator pole width b_{sp}. After investigating F_d as a function of l_m and b_{sp}, the optimum ratios of l_m/τ_p and b_{sp}/τ_p are determined. Figure 5 depicts the force density F_d investigated as a function of the stator pole width b_{sp} and the magnet length l_m. Maximum force densities F_d at different l_m/τ_p and b_{sp}/τ_p ratios are marked with circles in Figure 5.

(6) The magneto-motive force mmf by current and the air-gap length l_g are fixed to 3000 [AT] and 1 [mm], respectively. The magnet length l_m and the stator pole width b_{sp} are fixed using the optimum ratios of l_m/τ_p and b_{sp}/τ_p determined in the previous progress. Force

densities F_d of the machine are calculated as a function of the pole pitch τ_p in order to determine the optimum size of τ_p. Figure 6 depicts the force density F_d investigated as a function of the pole pitch τ_p.

(7) Force densities F_d of the machine are calculated as a function of the magneto-motive force mmf by current in order to determine the optimum value of mmf. Figure 7 depicts the force density F_d as a function of the magneto-motive force mmf for a TFPM machine with $l_g = 5$ [mm], $\tau_p = 50$ [mm]. Considering the saturation effect of the machine, it seems a better choice to determine the mmf at 10,000 [Ampere-turn] that is multiplication of 2×10^6 [Ampere/m] and air-gap length l_g [m].

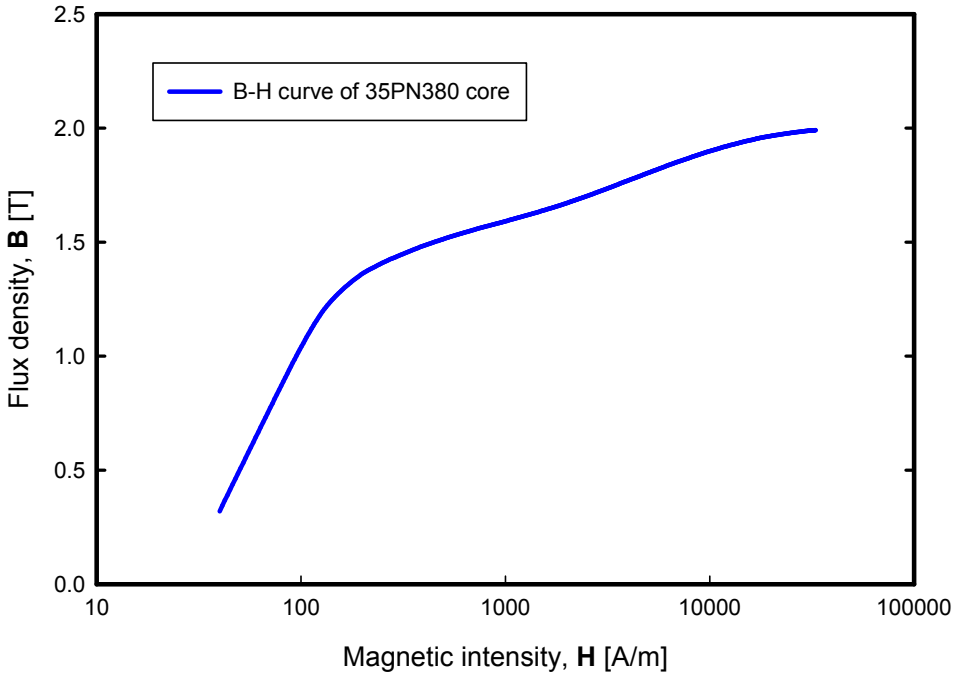

Figure 4: *Flux density and magnetic field intensity (B-H) curve of the iron core used in the analysis model*

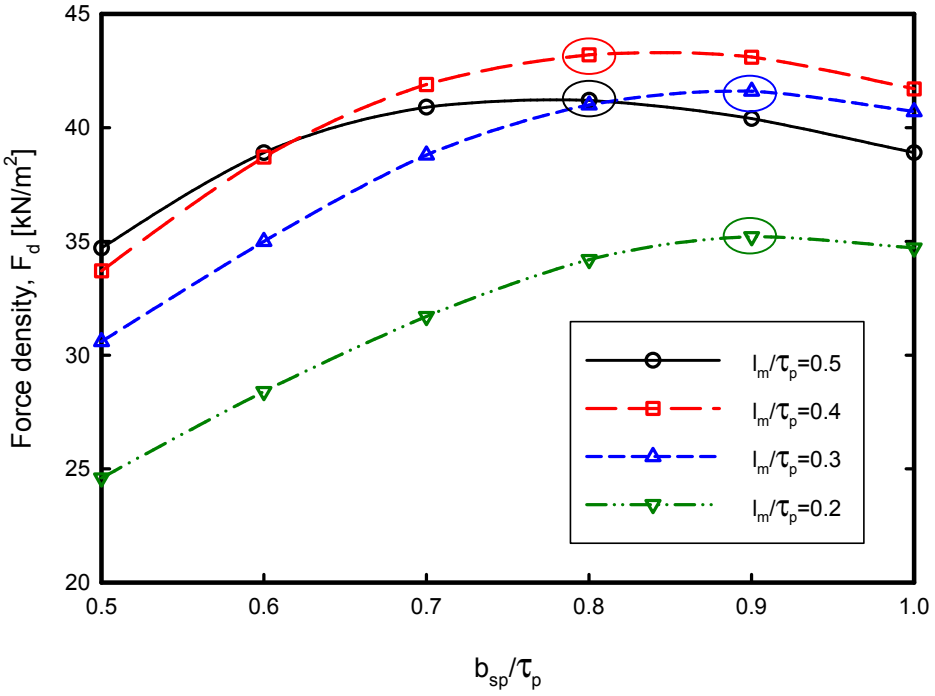

Figure 5: *Force density F_d as a function of the ratios of PM length l_m to pole pitch τ_p, and stator pole width b_{sp} to pole pitch τ_p*

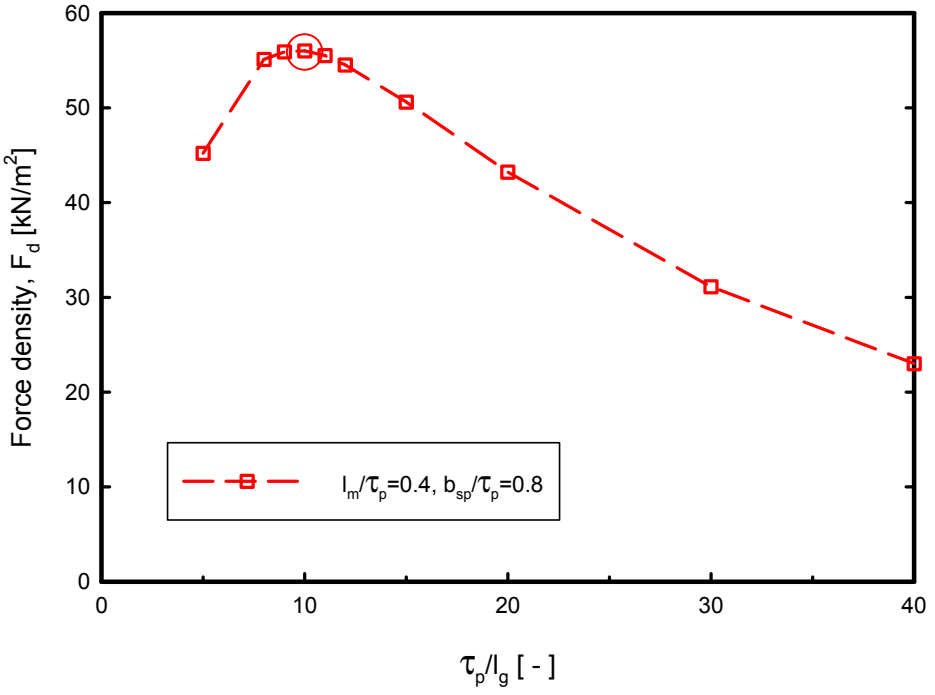

Figure 6: *Force density F_d as a function of pole pitch τ_p*

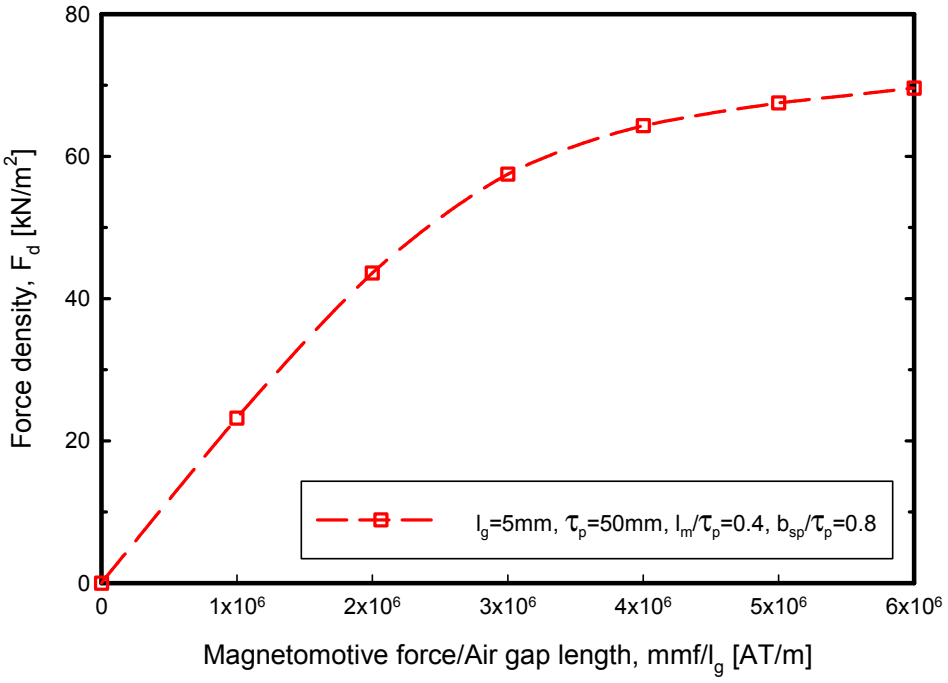

Figure 7: *Force density of a TFPM machine with $l_g = 5$ [mm] and $\tau_p = 50$ [mm] F_d as a function of the mmf by current*

From the FEA results represented in Figures 5, 6 and 7, the following is taken:

- The air-gap length is a main parameter in the electromagnetic design of TFPM machines.
- The optimum pole pitch is determined by $\tau_p = 10 l_g$.
- The optimum magnet length is determined by $l_m = 0.4\tau_p$.
- The optimum stator pole width is determined by $b_{sp} = 0.8\tau_p$.
- The optimum magneto-motive force by current mmf is determined by $mmf[AT] = N_s I_s = 2000000[AT/m] \times l_g[m]$.

In order to achieve the maximum force density of TFPM machines under the limited design condition, electromagnetic dimensions and parameters of TFPM machines are determined in TABLE 2.

TABLE 2
PARAMETERS AND DIMENSIONS OF TFPM MACHINES

Air gap diameter (Generator rotor diameter)	$D_{g.TFPMG} = D_{g.RFPMG}$ [m]
Air gap length	$l_g = \frac{D_g}{1000}$ [m]
Pole pitch	$\tau_p = 10 l_g$ [m]
Ratio of magnet height to pole pitch	$l_m / \tau_p = 0.4$ [-]
Magnet height	$l_m = l_m / \tau_p \times \tau_p$ [m]
Ratio of stator pole width to pole pitch	$b_p / \tau_p = 0.8$ [-]
Stator pole width	$b_p = b_p / \tau_p \times \tau_p$ [m]
Rotor pole width	$b_{pr} = \tau_p - l_m$ [m]
Magneto-motive force mmf by current	$mmf = N_{cslot} I_s = 2000000 \times l_g$ [AT]
Current density	$J_s = 3$ [A/mm^2]
Number of conductors per slot	$N_{cslot} = N_{cslot} I_s / I_s$ [-]
Cross-section area of conductors per slot	$A_{Cu1ph} = \frac{N_{cslot} I_s}{10^6 \cdot J_s}$ [m^2]
Slot filling factor	$k_{sfill} = 0.65$ [-]
Cross-section area of slot	$A_s = A_{Cu1ph} / k_{sfill}$ [m^2]
Stator slot width	$b_s = \sqrt{A_s}$ [m]
Stator slot height	$h_s = b_s$ [m]
Number of pole pairs	$p = \frac{\pi D_g}{2\tau_p}$ [-]
Stator pole length	$l_{sp} = \frac{e_{p.\max}}{p \omega_e N_{cslot} B_{p\max} b_p}$ [m]
Stator height	$h_S = h_{sy} + h_s + h_R$ [m]
Stator yoke height	$h_{sy} = h_{st}$ [m]
Rotor height	$h_R = l_{sp}$ [m]
Air gap area	$A_g = \pi D_g l_s$ [m^2] Here, $l_s = m\left(2l_{sp} + b_s\right)$ [m^2]

3. Generalization of magnetic circuit of PM machines

3.1 Linear model

In electric machines it is generally necessary to establish flux between a stationary part and a moving part. This involves causing flux to cross an air gap. To produce a strong magnetic field in an air gap, permanent magnet (PM) materials are being used for electric machines [6]. In the research of this thesis, PM machines are thus considered for use in generators of large direct-drive wind turbines. In order to show how to model the magnetic circuit and how to calculate the flux of PM machines, a generalized configuration of the magnetic circuit is given as Figure 8.

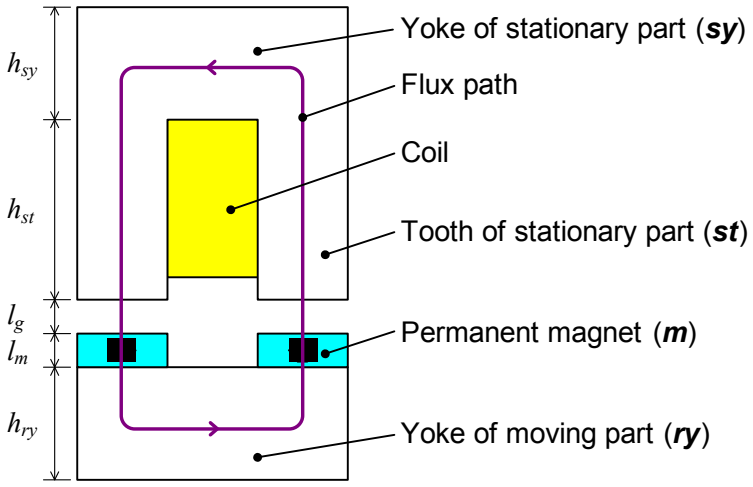

Figure 8: *Cross-section of a simplified magnetic circuit of a PM machine*

In Figure 8 h_{sy} is the height of yoke of the stationary part, h_{st} is the height of the tooth of the stationary part, l_g is the length of air gap, l_m is the height of the magnets and h_{ry} is the height of the yoke of the moving part. A flux path caused by the magnets is represented by a bold line with arrows. This path is used as a contour of the magnetic circuit to apply Ampere's circuit law. The contour is used to calculate the flux density due to the permanent magnets in the air gap and the iron cores.
An equation for the B-H characteristic of the magnets in the second quadrant is given as

$$B_m = \mu_0 \mu_{rm} H_m + B_{rm} \quad (1)$$

where, B_m is the flux density of the magnets [T], μ_0 is the permeability of free space [H/m], μ_{rm} is the recoil permeability of the magnets [-], H_m is the magnetic field intensity of the magnets [A/m] and B_{rm} is the remanent flux density of the magnets [T].

Equations for the B-H characteristic of the air gap and iron cores are written as (2), (3), (4) and (5), respectively.

$$B_g = \mu_0 H_g \quad (2)$$

$$B_{ry} = \mu_0 \mu_{r.ry} H_{ry} \quad (3)$$

$$B_{st} = \mu_0 \mu_{r.st} H_{st} \quad (4)$$

$$B_{sy} = \mu_0 \mu_{r.sy} H_{sy} \quad (5)$$

B is the flux density [T], H is the magnetic field intensity [A/m] and μ_r is the relative permeability [-]. The subscripts of g, ry, st and sy represent the air gap, the yoke of the moving part, the tooth of the stationary part and the yoke of the stationary part, respectively.

Using Ampere's circuit law, the contour in Figure 8 is expressed as

$$2H_g l_g + 2H_m l_m + H_{ry} l_{ry} + 2H_{st} l_{st} + H_{sy} l_{sy} = 0 \quad (6)$$

where l is the magnetic field length.

At low values of the magnetic field intensity, the flux density in iron cores increases almost linearly. The permeability of iron cores with low magnetic intensity is much larger than the permeability of the air and the magnets. Therefore, (6) can be simplified by neglecting terms of the magnetic field intensity of iron cores for the range of low magnetic field intensity as

$$2H_g l_g + 2H_m l_m = 0 \quad (7).$$

From the continuity of flux, the flux ϕ is written as

$$\phi = B_g A_g = B_m A_m = B_{ry} A_{ry} = B_{st} A_{st} = B_{sy} A_{sy} \quad (8)$$

where A is the area.

In order to calculate the flux density in the air gap, (7) is reformulated as (9) using (1), (2) and (8).

$$2\frac{B_g}{\mu_0} l_g + 2\frac{B_g \dfrac{A_g}{A_m} - B_{rm}}{\mu_0 \mu_{rm}} l_m = 0 \quad (9)$$

Therefore, the air gap flux density is determined by (10).

$$B_g = \frac{2B_{rm} l_m}{\mu_0 \mu_{rm}} \times \frac{1}{\dfrac{2l_g}{\mu_0} + \dfrac{2A_g l_m}{\mu_0 \mu_{rm} A_m}} \quad (10)$$

Assuming that the flux ϕ varies sinusoidally with time, the flux ϕ [Wb], the flux linkage λ [Wb-turns] and the no-load phase voltage e [V] thus are expressed as (11), (12) and (13).

$$\phi(t) = \phi_{\max} \sin \omega_e t \quad (11)$$

where ϕ_{max} is the amplitude of the flux [Wb], ω_e is the angular frequency (= $2\pi f$, here f is the frequency) [rad/s] and t is time [s].

From the equations expressed above and Faraday's law, the flux linkage λ and the no-load voltage e are given as

$$\lambda = N_s \phi \quad (12)$$

$$e = \frac{d\lambda}{dt} \quad (13)$$

where N_s is the total number of windings per phase [turns].

The no-load phase voltage induced in the N_s turns coil with time is written as

$$e(t) = N_s \frac{d\phi}{dt} \quad (14).$$

(14) is reformulated by substituting (11) into (14) as

$$e(t) = N_s \phi_{\max} \omega_e \cos \omega_e t = \hat{e} \cos \omega_e t \quad (15).$$

The amplitude of the no-load phase voltage is given as

$$\hat{e} = N_s \phi_{\max} \omega_e = \lambda_{\max} \omega_e \quad (16).$$

Generator power is formulated as a function of the number of phases m [-], the terminal voltage V_t [V], the nominal current I_{snom} [A] and the power factor $\cos\phi$ [-] as

$$P = m V_t I_{snom} \cos\phi \quad (17).$$

This chapter focuses on the electromagnetic design of generators, and the power factor $\cos\phi$ is assumed as 1 (one) in the analytical modelling. The equation of generator power is re-formulated as

$$P = m E I_{snom} \quad (18).$$

Here, E is the root-mean-square (RMS) value of the no-load phase voltage. The minimum nominal current I_{snom} necessary to produce the power of a three-phase electric machine is written by

$$I_{snom} = \frac{P}{3E} \quad (19)$$

The no-load phase voltage of a surface-mounted RFPM machine is formulated as

$$E = \frac{2}{\sqrt{2}} k_w N_{cslot} p \omega_m r_g l_s B_{g.\max} \quad (20)$$

where k_w is the winding factor, N_{cslot} is the number of conductors per a slot, p is the number of pole pair, ω_m is the mechanical angular velocity, r_g is the radius of generator rotor, l_s is the stack length in axial direction, and $B_{g.\max}$ is the amplitude of air-gap flux density.

Electromagnetic analysis models and relevant expressions on TFPM machines have been discussed and formulated by a number of authors as discussed in [7]. However, most models and equations are not sufficient for use with various topologies of TFPM machines because of restrictiveness of the models and equations. Therefore, in this thesis a generalized formulation of no-load phase voltage of TFPM machines is developed and proposed as

$$E = \left(\frac{\pi b_p}{\sqrt{2}\tau_p} \right) N_{cslot} p \omega_m r_g l_{sp} B_{p.\max} \quad (21)$$

where b_p is the pole width, τ_p is the pole pitch, l_{sp} is the pole length in axial direction, and $B_{p.\max}$ is the amplitude of flux density in the pole.

3.2 Nonlinear model

When the magnetic field intensity H in iron cores is increased, their flux density increases nonlinearly, which leads to a decrease in the permeability of the iron cores. Further increasing the magnetic field's intensity results in the iron cores being saturated and an increase in the reluctances of the magnetic path. Therefore, it is necessary to consider the nonlinear

characteristic of the flux density of the iron cores when designing electric machines meant to operate in the region of higher flux density.

The flux caused by the magnets was calculated as (8) from the continuity of flux. The flux caused by the magnets is also calculated as a function of the magnetic field intensity of the magnets H_m, the magnetic field length of the magnets l_m and the total reluctance in the equivalent circuit R_t as (22).

$$\phi = \frac{H_m l_m}{R_t} \qquad (22)$$

The equivalent circuit of the magnetic reluctance of the model shown in Figure 8 could be simplified as Figure 9. In the figure, the white rectangles represent the iron core reluctances, the white rectangles with bold lines represent the air gap reluctances. The rectangles hatched represent the magnet reluctances.

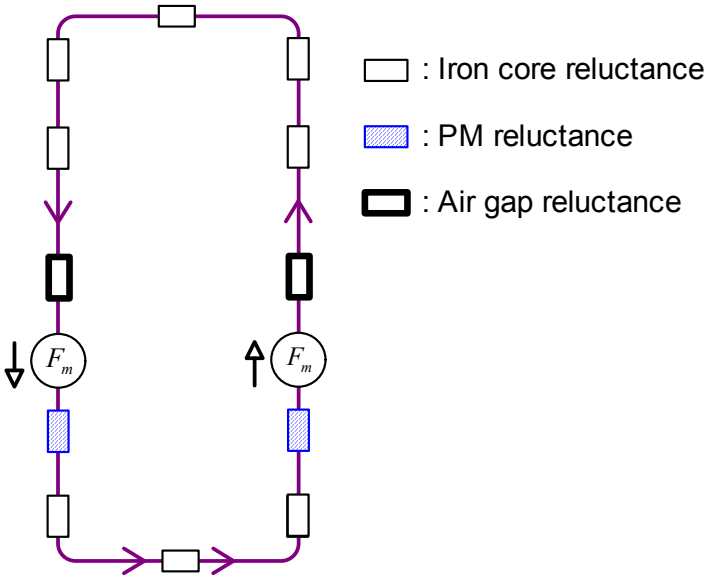

Figure 9: *A simplified equivalent reluctance model of* Figure 8

The total magnetic reluctance of the magnetic circuit of the model is given by

$$R_t = R_g + R_m + R_{ry} + R_{st} + R_{sy} \qquad (23)$$

where R_g is the reluctance of the air gap, R_m is the reluctance of the magnets, R_{ry} is the reluctance of the yoke of the moving part, R_{st} is the reluctance of the tooth of the stationary part and R_{sy} is the reluctance of the yoke of the stationary part.

General expressions of the magnetic reluctances are given as a function of the magnetic field length, its permeability and area.

$$R_g = \frac{2l_g}{\mu_0 A_g} \qquad (24)$$

$$R_m = \frac{2l_m}{\mu_m A_m} \qquad (25)$$

$$R_{ry} = \frac{l_{ry}}{\mu_{ry} A_{ry}} \quad (26)$$

$$R_{st} = \frac{l_{st}}{\mu_{st} A_{st}} = \frac{2h_{st}}{\mu_{st} A_{st}} \quad (27)$$

$$R_{sy} = \frac{l_{sy}}{\mu_{sy} A_{sy}} \quad (28)$$

Considering the nonlinear B-H characteristic of the iron cores and the above expressions, the flux density in the air gap B_g is reformulated as

$$B_g = \frac{H_m l_m}{R_t A_g} \quad (29)$$

From the continuity of flux, it is possible to calculate the flux density in the magnets B_m, the yoke of the moving part B_{ry}, the tooth of the stationary part B_{st} and the yoke of the stationary part B_{sy}. After determining the flux density in the air gap, the procedure and the expressions to calculate the flux ϕ, the flux linkage λ and the no-load voltage e are the same with as in section 3.1.

The procedure to determine the flux density, the flux, the flux linkage and the no-load induced voltage of a magnetic circuit including nonlinear characteristic is made as the following steps. Figure 10 depicts a flow chart of the procedure.

(Step1) Input predefined parameters of PM machines

(Step2) Determine the initial values of the flux densities of the air gap B_g, the magnets B_m, the yoke of the moving part B_{ry}, the tooth of the stationary part B_{st} and the yoke of the stationary part B_{sy} using Ampere's circuit law and the continuity of flux

(Step3) Assume the initial value of the permeability of the tooth of the stationary part μ_{st}. In the thesis we assume $\mu_{st} = 300\mu_0$ as an initial value.

(Step4) Calculate the magnetic field intensity of the tooth of the stationary part H_{st} by $H_{st} = \frac{B_{st(Step2)}}{\mu_{st(Step3)}}$.

(Step5) Re-calculate the flux density of the tooth of the stationary part B_{st} with the B-H curve of the iron core $B_{st} = f(H_{st}, BH-curve)$. Re-calculate the flux densities of the yoke of the moving part B_{ry} and the yoke of stationary part B_{sy} from the continuity of flux.

(Step6) Re-calculate the permeability of the tooth of the stationary part μ_{st} by $\mu_{st} = \frac{B_{st}}{H_{st}}$. Calculate the permeability of the yoke of the moving part μ_{ry} and the yoke of the stationary part μ_{sy}.

(Step7) Calculate the total reluctance of the magnetic circuit R_t by $R_t = R_g + R_m + R_{ry} + R_{st} + R_{sy}$.

(Step8) Calculate the flux ϕ by $\phi = \frac{H_m l_m}{R_t}$.

(Step9) Re-calculate the flux density of the tooth of the stationary part B_{st} by $B_{st} = \frac{\phi}{A_{st}}$ using ϕ calculated in *(Step8)*.

(Step10) Re-calculate the magnetic field intensity of the tooth of the stationary part H_{st} by $H_{st} = \frac{B_{st(Step9)}}{\mu_{st(Step6)}}$.

(Step11) Re-calculate the flux density of the tooth of the stationary part B_{st} with the B-H curve of the iron core $B_{st} = f(H_{st(Step10)}, BH - curve)$.

(Step12) Compare B_{st} calculated in *(Step9)* with B_{st} calculated in *(Step11)*. If $\left|B_{st(Step11)} - B_{st(Step9)}\right| \le accuracy$, then proceed to the next step. If not, go back to *(Step 6)*.

(Step13) Re-calculate the flux densities of the air gap B_g, the magnets B_m, the yoke of the moving part B_{ry} and the yoke of the stationary part B_{sy} using the continuity of flux.

(Step14) Re-calculate the flux ϕ, and calculate the flux linkage λ and the no-load induced voltage e.

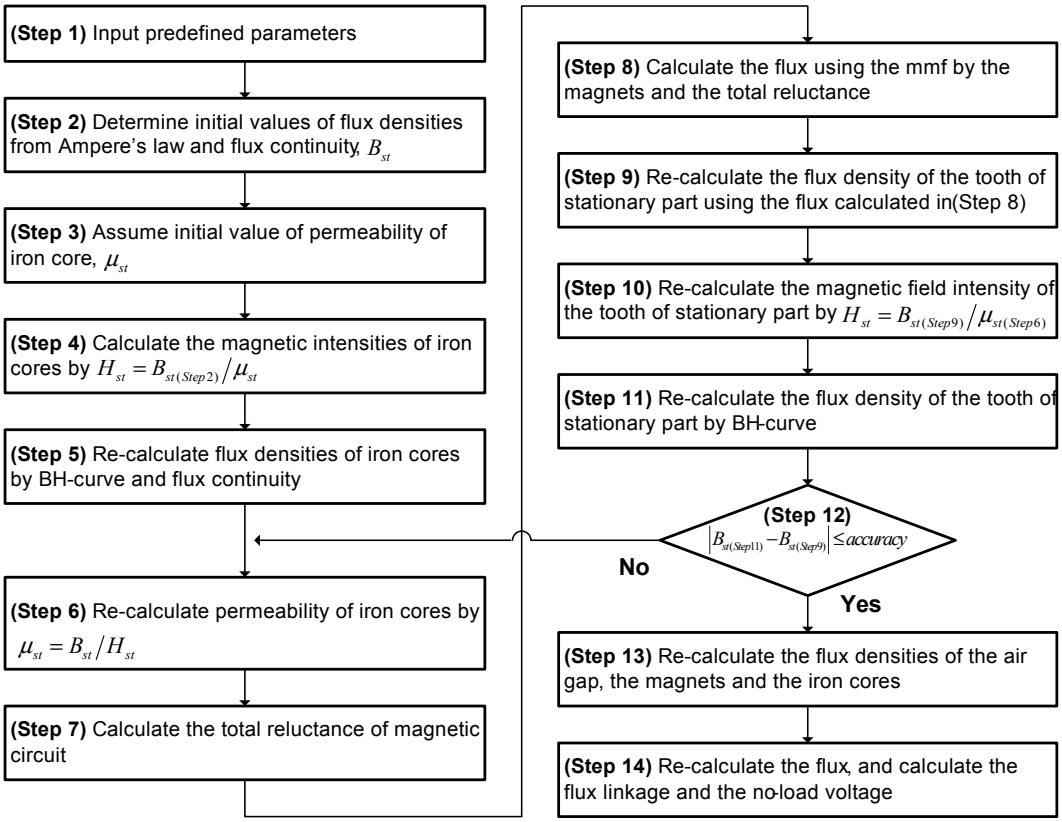

Figure 10: *Flow chart showing the process to determine the flux density, the flux, the flux linkage and the no-load induced voltage of the magnetic circuit of a PM machine*

3.3 Magnetic circuit modelling of PM machines

3.3.1 RFPM machine

In this section, a contour is sketched to which Ampere's circuit law is applied as shown in Figure 11. The figure depicts two poles of the magnetic circuit of a surface-mounted RFPM machine, which consists of a stator with slotted iron cores and full pitch windings, and a rotor with iron cores and magnets.

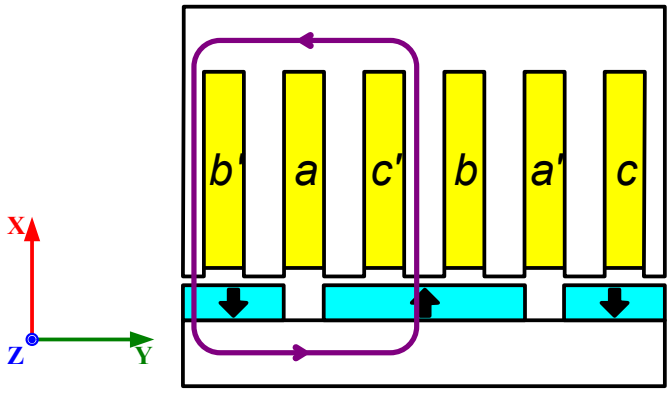

Figure 11: *The contour of a surface-mounted RFPM machine to apply Ampere's circuit law*

In the modelling of the magnetic circuit of the RFPM machine, it is assumed that

- the flux density crosses the magnets and the air gap perpendicularly
- there is no leakage flux in the circuit
- the fluxes in the air gap, the magnets, the rotor yoke, the stator teeth and the stator yoke are equal.

In order to fulfill the above assumptions, the shape of the magnets is modified from Figure 11 to Figure 12. In Figure 12, the flux paths in a contour are represented with lines and arrows. A simplified equivalent circuit of the magnetic reluctance of the RFPM machine illustrated in Figure 11 and Figure 12 is the same with the equivalent circuit shown in Figure 9.

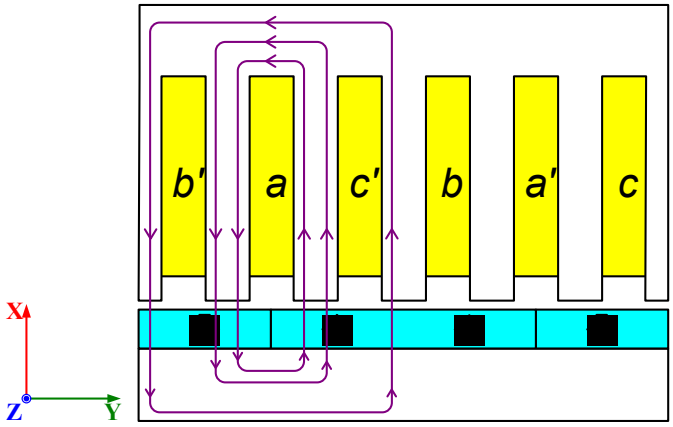

Figure 12: *A linearized RFPM machine with the modified magnets and the flux paths*

3.3.2 TFPM machine

Figure 13 depicts a flux-concentrating TFPM machine with five poles and a contour to which Ampere's circuit law is applied. The machine consists of a stator with iron cores and windings, a rotor with flux-concentrating iron cores and the magnets. A simplified equivalent circuit model of the magnetic reluctances of the TFPM machines is illustrated in Figure 14.

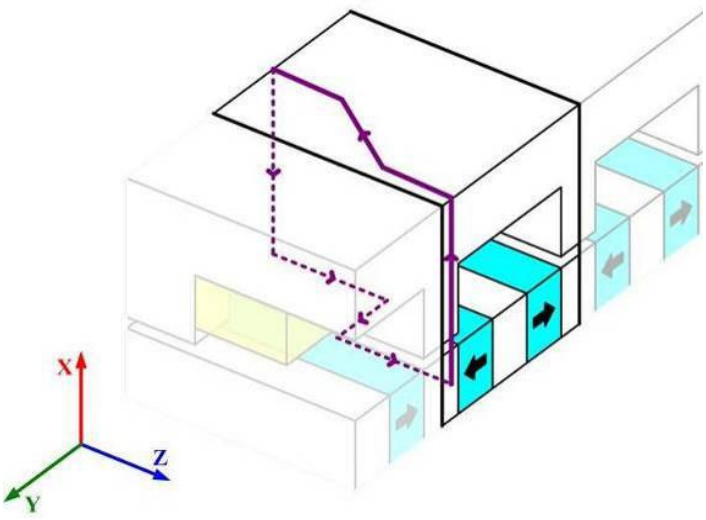

Figure 13: *The contour of a flux-concentrating TFPM machine to apply Ampere's circuit law*

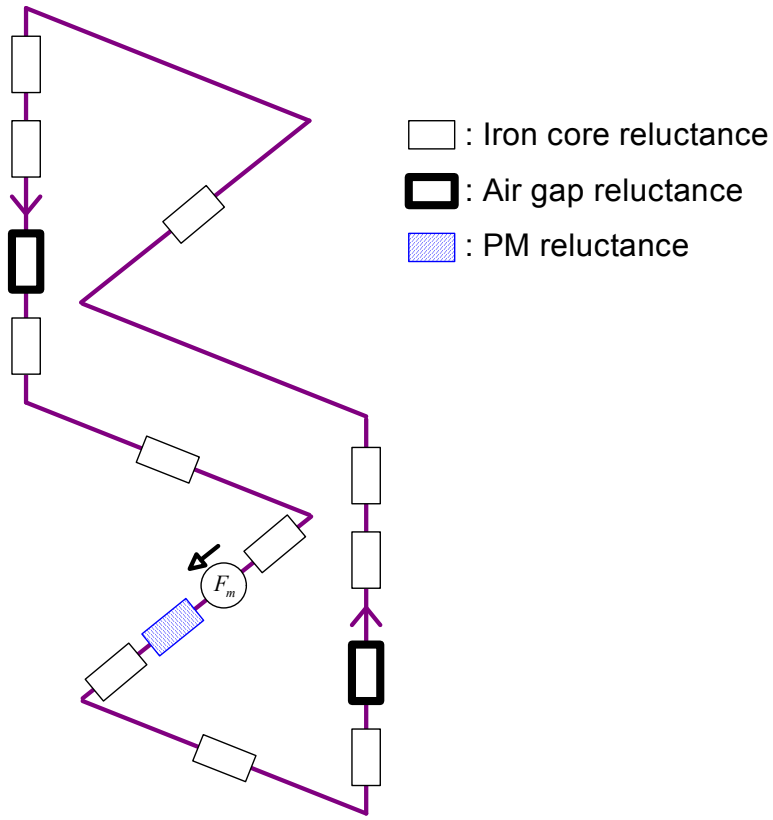

Figure 14: *A simplified equivalent circuit of magnetic reluctances of flux-concentrating TFPM machines*

In the equivalent circuit of the TFPM machine, the leakage fluxes of TFPM machines are much larger than the leakage fluxes of the RFPM machines with full pitch windings. Therefore, the leakage fluxes of TFPM machines are included in the equivalent circuit in the thesis. Electromagnetic characteristics of the TFPM machines are the same and repetitive in every one pole pair. Therefore, the electromagnetic equivalent circuit of one pole pair is considered for the analytical model. The equivalent circuit including the leakage fluxes is illustrated in Figure 15, which is made by cutting the stator in the middle and spreading both the stator and the rotor. The white rectangles are the iron core reluctances and the white rectangles with bold lines are the air gap reluctances. The blue rectangles hatched are the PM reluctances and the red rectangles dotted are the leakage flux reluctances.

In the modelling of the magnetic circuit of the TFPM machine, it is assumed that

- the flux density crosses the magnets perpendicularly
- the flux density crosses the air gap on iron cores perpendicularly
- the leakage fluxes are modelled as shown in Figure 15.

The equivalent circuit is modified as Figure 16 including the fluxes and the magneto-motive force due to the magnets. In order to determine the fluxes ϕ_A, ϕ_B, ϕ_C, ϕ_D, ϕ_E, ϕ_F, ϕ_G, ϕ_H, ϕ_I, ϕ_J, ϕ_K and ϕ_L in Figure 16 (a), Kirchhoff's voltage law is applied to the fluxes Φ_1, Φ_2, Φ_3, Φ_4 and Φ_5 in Figure 16 (b), (c), (d) and (e).

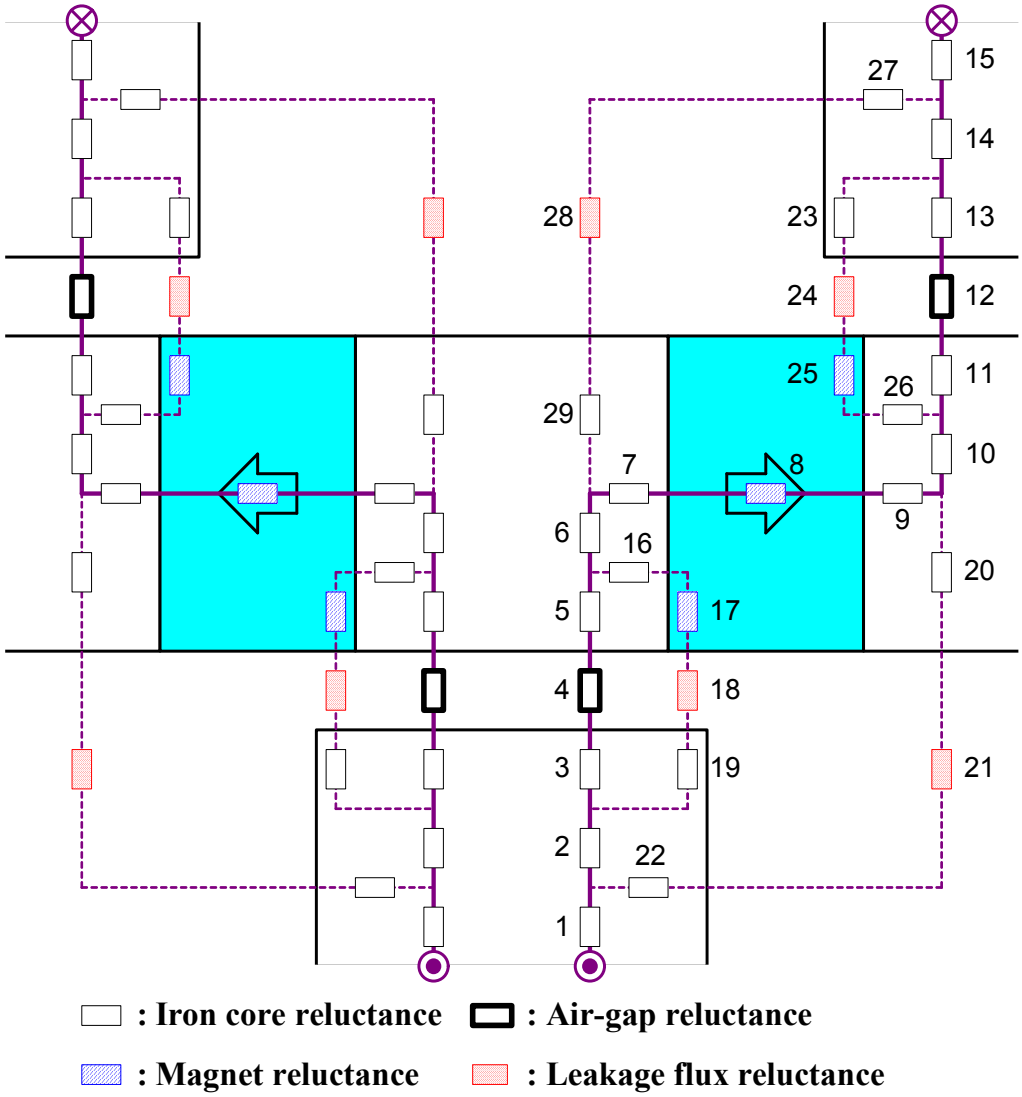

Figure 15: *Equivalent circuit of magnetic reluctances of flux-concentrating TFPM machines including leakage flux reluctances*

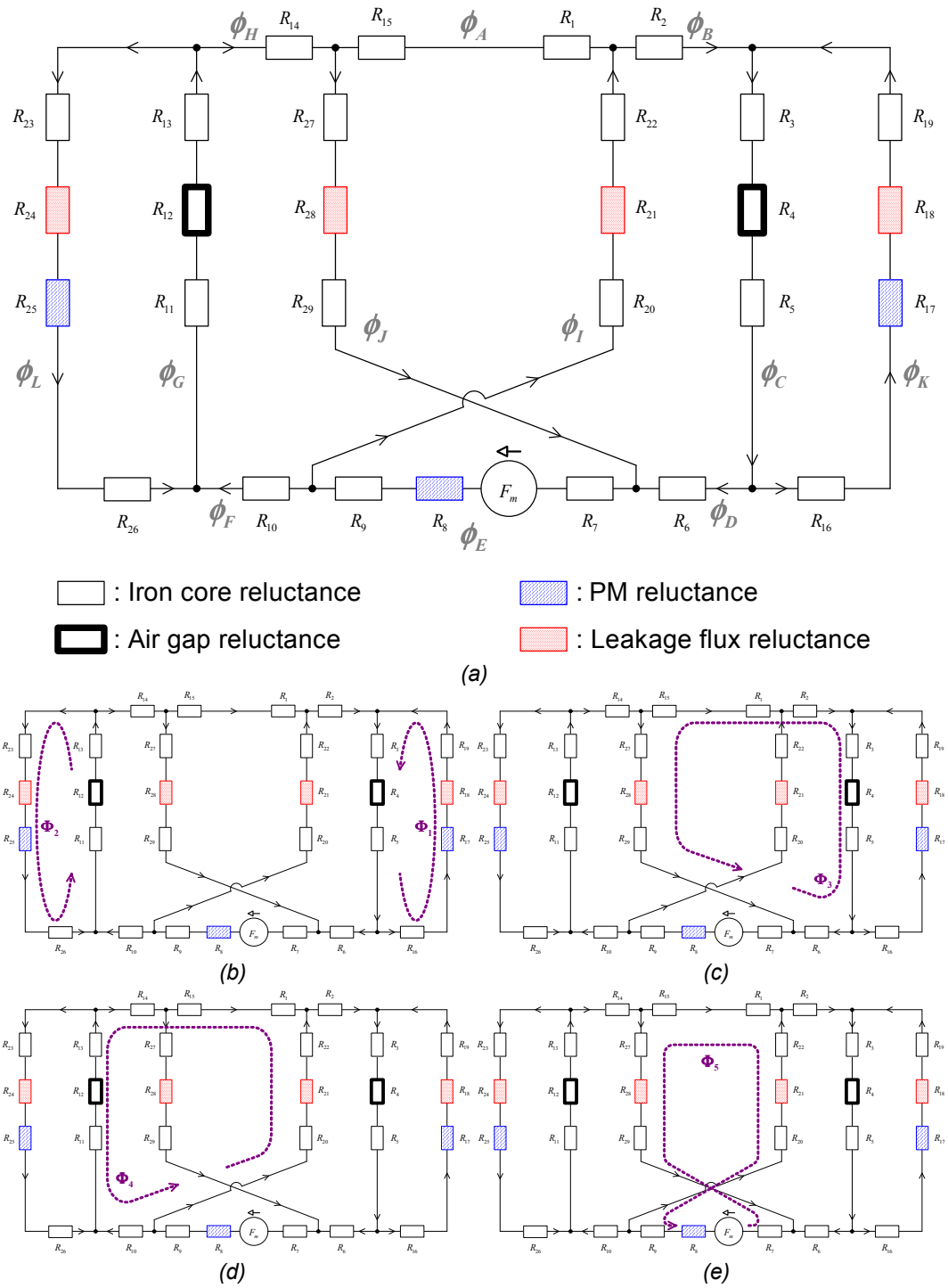

Figure 16: *Equivalent circuit of magnetic reluctances of flux-concentrating TFPM machines including leakage flux reluctance and magneto-motive force caused by magnets*

4. Verification of magnetic circuit analysis model

This section discusses the verification of the proposed analysis model of TFPM machines for two cases, no-load case and load case. In order to verify the analysis model for no-load case, the no-load induced voltage obtained from the analysis model is compared with the no-load voltage determined from the finite element analysis (FEA) and the measurement. To validate the proposed analysis model for load case, the force obtained from the analysis model is compared with the force obtained from the FEA. The TFPM machine considered for the verification is a single-sided, single-winding flux concentrating TFPM machine with U-core and passive rotor as illustrated in Figure 17. Solid iron cores are used to build the TFPM machine for easier manufacturing.

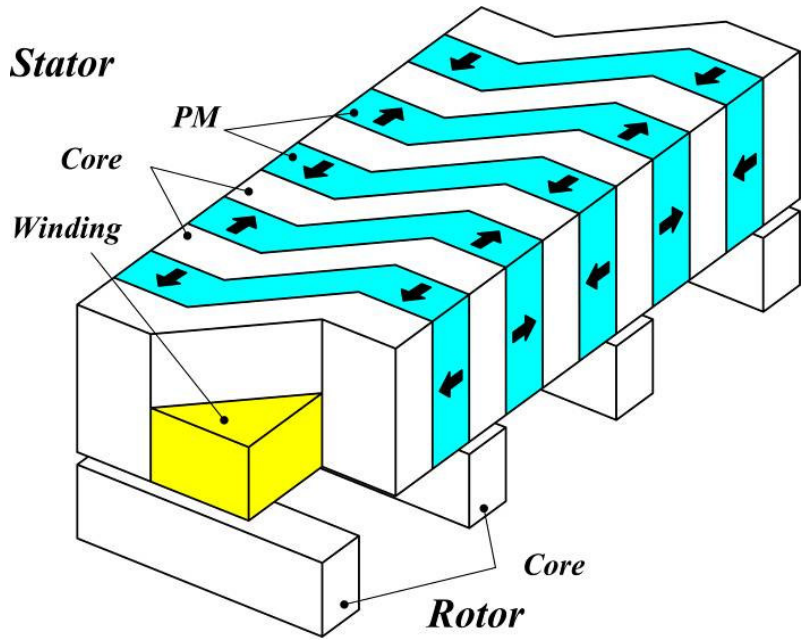

Figure 17: *A linearized single-sided single-winding flux concentrating TFPM machine with U-core and passive rotor*

4.1 Verification of no-load case

4.1.1 Analysis model

Analysis models and formulations in the previous chapter are used for the analysis of the single-sided, single-winding flux concentrating TFPM machine with U-core and passive rotor. The equivalent circuit of magnetic reluctances of the TFPM machine in Figure 17 is represented by cutting the rotor in the middle and spreading both the stator and the rotor as Figure 18.
Material characteristics of the TFPM machine are given in TABLE 3. The parameters and dimensions of the single-sided, single-winding flux concentrating TFPM machine with U-core and passive rotor is given in TABLE 4. Figure 19 depicts the characteristics of the flux density and the magnetic intensity of the solid iron cores used for the TFPM machine.
The amplitudes of the flux density in the stator core between magnets, and the flux, the flux linkage and the no-load induced voltage per a pole pair obtained by the analysis are given in TABLE 5.

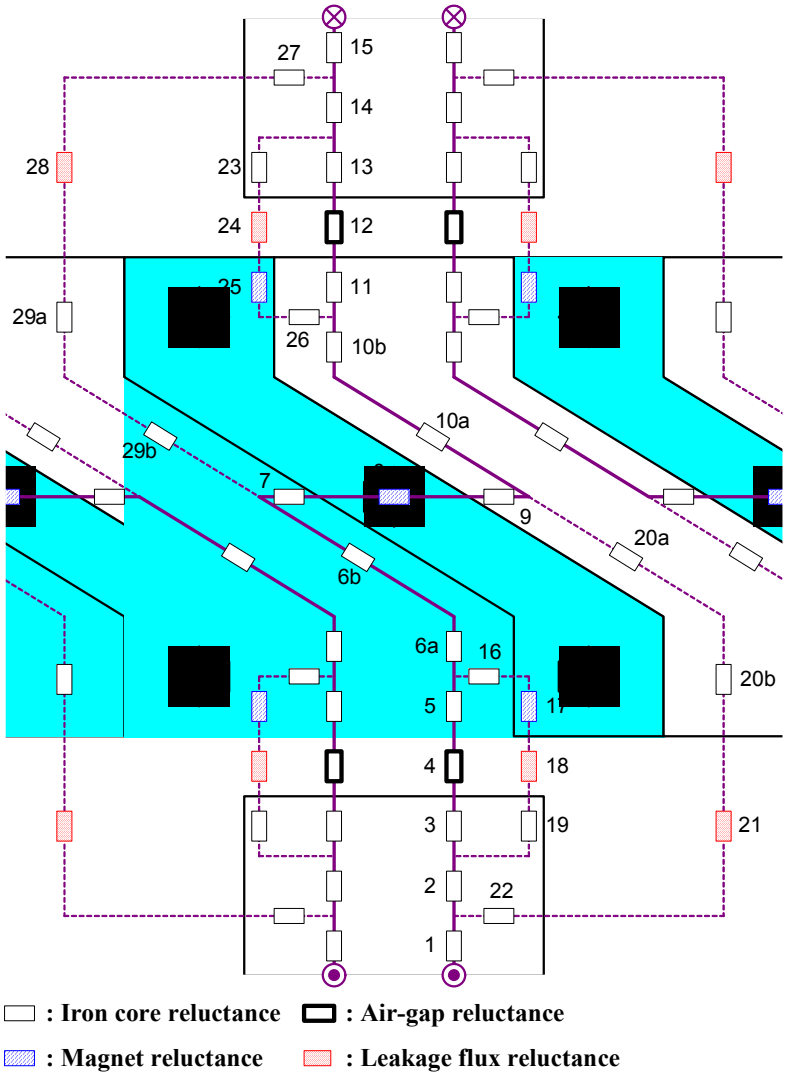

Figure 18: *Equivalent circuit of magnetic reluctances of single-sided single-winding flux concentrating TFPM machine with U-core and passive rotor*

TABLE 3
MATERIAL CHARACTERISTICS OF TFPM MACHINE

Iron core type		Solid core (S20c) B-H curve: see **Figure 19**
Resistivity of copper, ρ_{Cu}		0.025 [μΩm]
Remanent flux density of permanent magnets, B_{rm}		1.3 [T]
Relative recoil permeability of permanent magnets, μ_{rm}		1.06 [-]
Permeability of free space, μ_0		$4\pi\times10^{-7}$ [H/m]
Density	Iron core, ρ_{Fe}	7800 [kg/m^3]
	Permanent magnet, ρ_{pm}	7600 [kg/m^3]
	Copper, ρ_{Cumass}	8900 [kg/m^3]

TABLE 4
PARAMETERS AND DIMENSIONS OF TFPM MACHINE

Air gap length	$l_g = 2$ [mm]
Pole pitch	$\tau_p = 20$ [mm]
Magnet height	$l_m = 10$ [mm]
Stator pole width	$b_p = 14$ [mm]
Rotor pole width	$b_{pr} = 10$ [mm]
Number of conductors per slot	$N_{cslot} = 288$ [Turn]
Stator slot width	$b_s = 50$ [mm]
Stator slot height	$h_s = 35$ [mm]
Number of pole pair	$p = 7.5$ [-]
Stator pole length	$l_{sp} = 40$ [mm]
Stator height	$h_S = 75$ [mm]
Stator yoke height	$h_{sy} = 40$ [mm]
Rotor height	$h_R = 40$ [mm]

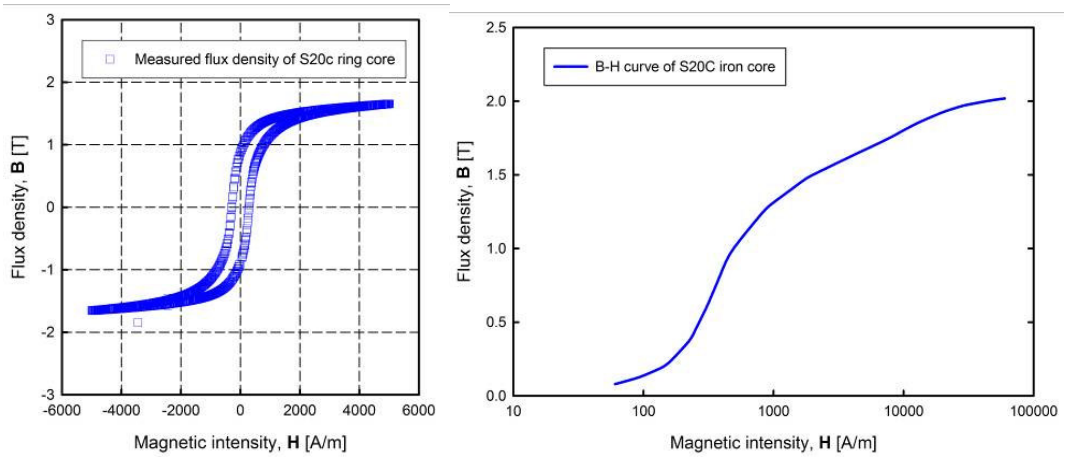

(a) B-H curve measured *(b) B-H curve used in the analysis*

Figure 19: *Flux density and magnetic intensity (B-H) curve of the iron core (S20c)*

TABLE 5
AMPLITUDES OF FLUX DENSITY, FLUX, FLUX LINKAGE AND NO-LOAD INDUCED VOLTAGE OF SINGLE-SIDED SINGLE-WINDING FLUX CONCENTRATING TFPM MACHINE WITH U-CORE AND PASSIVE ROTOR BY THE ANALYTICAL MODEL

Flux density in the stator core, $\hat{B}$	1.46 [T]
Flux in the stator core per a pole pair, $\hat{\phi}_{pole\_pair}$	0.000586 [Wb]
Flux linkage in the stator per a pole pair, $\hat{\lambda}_{pole\_pair}$	0.168665 [Wb]
No-load induced voltage per a pole pair, $\hat{e}_{pole\_pair}$	26.49 [V]

4.1.2 Finite element analysis

Figure 20 depicts two poles of the single-sided, single-winding flux concentrating TFPM machine with U-core and passive rotor for three-dimensional finite element analysis (3D FEA). TABLE 6 gives the amplitudes of the flux density, the flux, the flux linkage and the no-load induced voltage obtained by the 3D FEA.

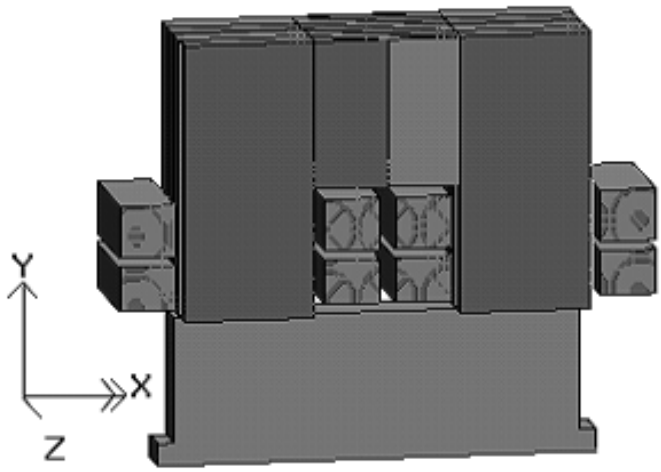

Figure 20: *3D FEA model for single-sided single-wind flux concentrated TFPM machine with U-core and passive rotor*

TABLE 6
AMPLITUDES OF FLUX DENSITY, FLUX, FLUX LINKAGE AND NO-LOAD INDUCED VOLTAGE OF SINGLE-SIDED SINGLE-WINDING FLUX CONCENTRATING TFPM MACHINE WITH U-CORE AND PASSIVE ROTOR BY 3D FEA

Flux density in the stator core, $\hat{B}$	1.35 [T]
Flux in the stator core per a pole pair, $\hat{\phi}_{pole\_pair}$	0.000540 [Wb]
Flux linkage in the stator per a pole pair, $\hat{\lambda}_{pole\_pair}$	0.155416 [Wb]
No-load induced voltage per a pole pair, $\hat{e}_{pole\_pair}$	24.41 [V]

4.2 Verification in the case with a load

To validate the proposed analysis model of the TFPM machine for the case with a load, the force obtained in the analysis model is compared with the force obtained through the 3D FEA. Using (18) and (21), the Lorenz force of a phase of the TFPM machine for the analysis model is formulated as

$$F = E\frac{I_{snom}}{v_g} = \left(\frac{\pi b_{sp}}{\sqrt{2}\tau_p}\right) pN_{cslot}B_{p.\max}l_{sp}v_g\frac{I_{snom}}{v_g} = \left(\frac{\pi b_{sp}}{\sqrt{2}\tau_p}\right) pN_{cslot}B_{p.\max}l_{sp}I_{snom} \quad (30)$$

The thrust force per pole pair of the TFPM machine obtained through the 3D FEA is represented in Figure 21 as a function of the rotor displacement.

Due to the effect of the cogging force and the reluctance force, the sinusoidal distribution of the thrust force of electric machines is distorted. The effect of the cogging force and the reluctance force in TFPM machines is noticeably high compared to longitudinal flux permanent magnet (LFPM) machines. Thus, the force distribution of the TFPM machine is not sinusoidal as shown in Figure 21.

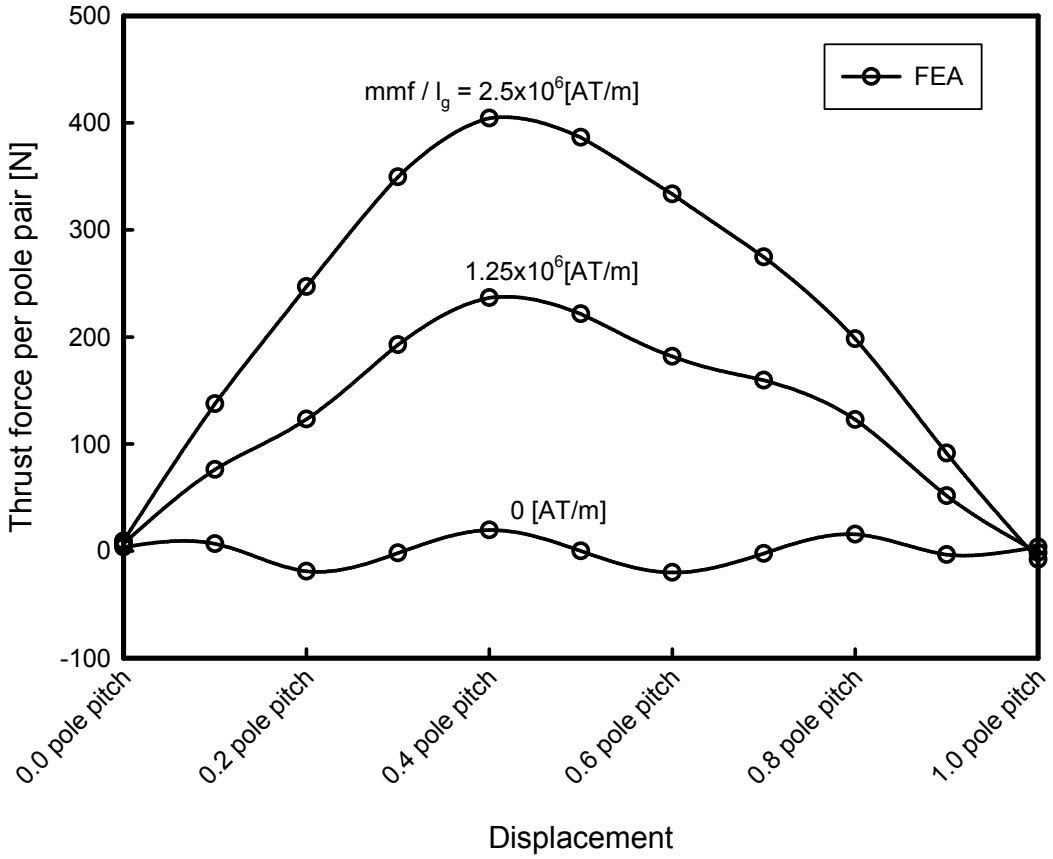

Figure 21: *Thrust force per pole pair obtained through 3D FEA and static force measurement*

The analytical model and the formulation (30) do not include the effect of the cogging and reluctance force in calculating the thrust force. Therefore, the following assumptions are also made to verify the analytical model of the TFPM machine in the case with a load.

- The force distribution obtained by the analytical model is sinusoidal.
- The force at the rotor displacement of 0.5 pole pitch is the maximum.
- In the force distribution obtained through the 3D FEA and the static force measurement, the cogging effect is omitted. Thus the force at the rotor displacement of 0.5 pole pitch is compared with the force obtained by both the analytical model and (30).

The peak thrust force obtained through the 3D FEA, the analytical model and the above assumptions is given as a function of the magnetomotive force per air gap length, $\boldsymbol{mmf/l_g}$ in TABLE 7. The peak force by the analytical model is compared with the peak force by the 3D FEA, and the comparison results are represented in Figure 22. At the rated magnetomotive force per air gap length, $\boldsymbol{mmf/l_g}$=2x10^6 [AT/m], the peak force obtained by the analytical model is 10 % larger than the force obtained by the 3D FEA. Increasing the $\boldsymbol{mmf/l_g}$, it becomes bigger that the differences between the force by the analytical model and the force by the 3D FEA, because the analytical model does not include the saturation effect by the stator current.

TABLE 7
THRUST FORCE PER A POLE PAIR OBTAINED THROUGH THE ANALYTICAL MODEL

	Magnetomotive force/Air gap length, mmf / l_g [AT/m]					
	0	0.63×10^6	1.25×10^6	1.88×10^6	2.5×10^6	3.1×10^6
F_{peak} by 3D FEA [N]		113.9	221.5	313.2	386.4	438.0
F_{peak} by analytical model [N]		114.3	229.3	344.1	458.6	573.2

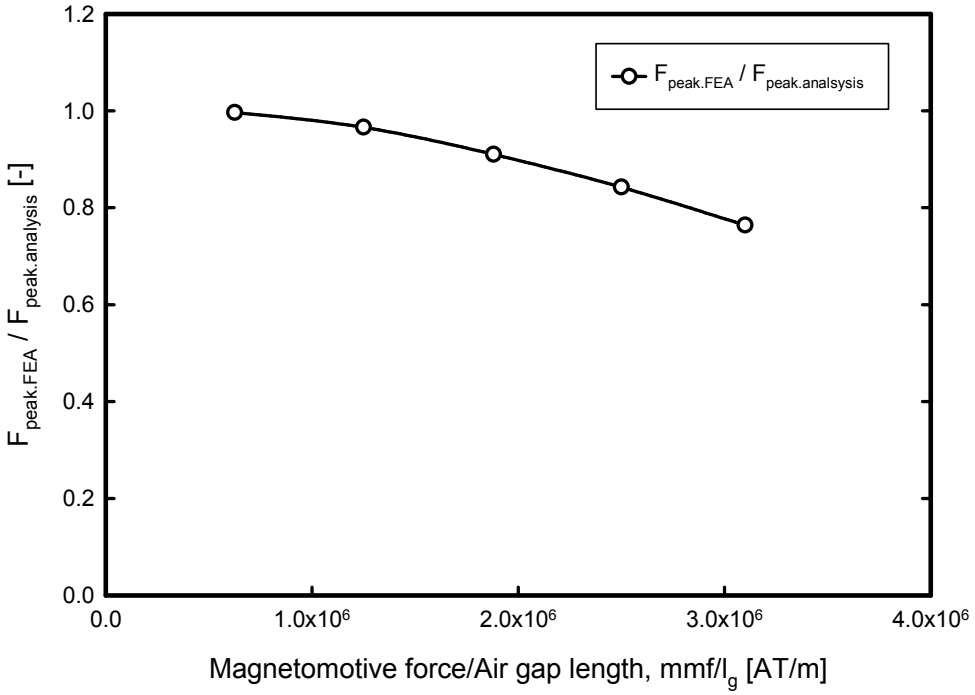

Figure 22: *Comparison of thrust force obtained by the 3D FEA, the measurement and the analytical model*

5. Conclusions

The main topic of discussion in this chapter was the development of a generalized analytical model for various topologies of permanent magnet (PM) machines. A slotted surface-mounted radial flux permanent magnet (RFPM) machine and flux-concentrating transverse flux permanent magnet (TFPM) machines were chosen in the modelling of these machines for direct-drive wind turbines.

Firstly, a determination of geometric parameters of RFPM machine and TFPM machine was discussed. For the RFPM machine, the geometric parameters were determined by an investigation of the parameters of RFPM machines discussed in scientific literature. To determine the geometric parameters of TFPM machines, two-dimensional finite element analyses (2D FEA) of electromagnetic fields were done. In the analyses it was focused on finding the optimum geometrical parameters to maximize the force density. The parameters to optimize were the magnet length, the stator pole width, the pole pitch and the magnetomotive force by current.

Next, generalized electromagnetic circuit analysis models were created for both the RFPM and TFPM machines. Nonlinear B-H characteristics of iron cores were included in the models. Leakage fluxes of TFPM machines are much larger than the RFPM machine with full pitch windings, thus the leakage fluxes were included in the models of TFPM machines.

Furthermore, to verify the analytical model of TFPM machines in no-load case, the no-load induced voltage obtained through the analytical model was compared with the no-load voltages obtained through the three-dimensional finite element analyses (3D FEA). The no-load voltage obtained by the analytical model at 1 m/s air gap speed was 8 % higher than the voltage obtained by the 3D FEA.
To validate the analytical model in the case with a load, the force obtained by the analytical model was compared with the force obtained through 3D FEA and the static force measurement as a function of the displacement and the stator current. At the nominal stator current, the force obtained by the analytical model is 10 % larger than the force obtained by the 3D FEA. Increasing the stator current larger than the nominal current, the difference between the force by the analytical model and the force by the 3D FEA becomes bigger. This was caused by no consideration of the saturation effect by the stator current in the analytical model.
The analytical models developed in this report will be used for a comparative design of PM wind generators in the final report (Deliverable No.: D 1B2.b.hp2). In the design the stator current will be limited to the nominal current.

References

[1] A. Grauers, “Design of direct-driven permanent-magnet generators for wind turbines”, Ph.D. dissertation, Chalmers University of Technology, Göteborg, Sweden, 1996.
[2] J.J. Cathey, “Electric machines: Analysis and design applying MATLAB”, McGraw-Hill, 2001.
[3] H. Polinder, F.F.A. van der Pijl, G.J. de Vilder, P. Tavner, “Comparison of direct-drive and geared generator concepts for wind turbines”, IEEE Trans. Energy Conversion, Vol. 21, pp. 725-733, September 2006.
[4] A.S. McDonald, M.A. Mueller and H. Polinder, “Comparison of generator topologies for direct-drive wind turbines including structural mass”, in Proc. of the International Conference on Electrical Machines(ICEM), pp. 360.1-7, September 2006.
[5] D. Bang, H. Polinder, G. Shrestha, and J.A. Ferreira, “Promising direct-drive generator system for large wind turbines”, EPE Journal, Vol. 13, pp. 7-13, September 2008.
[6] G.R. Slemon and X. Liu, “Modeling and design optimization of permanent magnet motors”, Elec. Mach. And Power Syst., Vol. 20, pp. 71-92, 1992.
[7] D. Bang, H. Polinder, G. Shrestha, and J.A. Ferreira, “Review of generator systems for direct-drive wind turbines”, in Proc. EWEC (European Wind Energy Conference & Exhibition), Brussels, Belgium, March 31 - April 3 2008.